Quantitative Binding Models for CYP2C9 Based on Benzbromarone Analogues[†]

Charles W. Locuson, II,[‡] Denise A. Rock,[§] and Jeffrey P. Jones*,[‡,§]

*School of Molecular Biosciences, Washington State University, Pullman, Washington 99164, and
Department of Chemistry, Washington State University, P.O. Box 644630, Pullman, Washington 99164-4630*

Received February 16, 2004; Revised Manuscript Received March 24, 2004

ABSTRACT: The cytochrome P450 (CYP) isoforms involved in xenobiotic metabolism are enzymes whose substrate selectivity remains difficult to predict due to wide specificity and dynamic protein−substrate interactions. To uncover the determinants of specificity for cytochrome CYP2C9, a novel library of benzbromarone (bzbr) inhibitors was used to reevaluate its pharmacophore. CoMSIA was used with the bzbr ligands to generate both quantitative binding models and three-dimensional contour plots that pinpoint predicted interactions that are important for binding to 2C9. Since this class of compounds is more potent than any other toward 2C9, the small molecule properties deemed most ideal by the software were used to address protein−ligand interactions using new mutagenesis and structural data. Nine new bzbr analogues provide evidence that specific electrostatic and hydrophobic interactions contribute the most to 2C9's specificity. Three of the new analogues are better isosteres of bzbr that contain bulky groups adjacent to the phenol and have increased pK_a values. These ligands test the hypothesis that anionic substrates bind with higher affinity to 2C9. Since they have higher affinity than the previous nonacidic analogues, the importance of bulky groups on the phenol ring appears to have been underestimated. CoMSIA models predict that these bulky groups are favorable for their hydrophobicity, while a negative charge is favored at the ketone oxygen rather than the phenol oxygen. The overlap of this ketone with electronegative groups of other 2C9 substrates suggests they act as key positive charge acceptors.

Xenobiotic oxidation in humans is catalyzed in large part by just a handful of cytochrome P450s (CYPs),[1] which are members of a superfamily of monooxygenases. These select isoforms function to transform generally small, lipophilic molecules such as drugs into more water soluble metabolites. One isoform, CYP2C9, contributes to the metabolism of nearly one-fifth of all drugs (*1*). This is significant because 2C9 has been implicated in potentially dangerous drug−drug interactions, which result from drugs competing for the same P450 (*2*, *3*). To prevent such problems, it would be advantageous to formulate predictive models for binding affinity, as well as other variables controlling pharmacokinetics.

The roadblock to such quantitative models is the increasingly evident role of both substrate and enzyme motion in determining P450 behavior (*4*, *5*). For instance, 2C9 has a preference for acidic substrates (*6*, *7*), but substrate affinity may depend on the population of distinct binding modes, the closing of the enzyme over the substrate after binding, and the size of the substrate. While large substrates have limited binding modes, some smaller substrates tumble freely and can be oxidized in multiple locations as a result (*8*).

Multiple substrates have also been shown to occupy the same binding pocket of some P450s simultaneously (*9*). Therefore, the precise properties giving rise to a P450's affinity for a new drug are not always evident without knowledge of closely related compounds.

Nevertheless, computational tools are capable of generating three-dimensional quantitative structure−activity relationships (3D-QSARs) for P450s (*10*−*13*). CoMFA is one such computational method that may be used to predict binding affinity; however, no such model based on the potent benzbromarone (bzbr) derivatives has been reported. The fact that bzbr is so potent (K_i = 19 nM) makes it an ideal probe for studying 2C9 behavior because the interactions it makes (or lacks) with 2C9 are most favored thermodynamically. To build the models, K_i values had to be determined for several new analogues, which were designed to test the role of pK_a and the positioning of different groups on the benzoyl ring. By using our previous 2C9 alignment rules, we established cross-validated CoMFA and CoMSIA models based on these novel bzbr derivatives (Figure 1). When the bzbr ligands were included with a more diverse data set, including warfarin, sulfaphenazole, and NSAID analogues, the model gained the depth to predict K_i values that span more than 4 orders of magnitude. In addition, the resulting pharmacophore appears to be a useful qualitative tool that explains the affinity of many of the 58 compounds in terms of their electrostatic, hydrophobic, and steric properties. The predicted enzyme−substrate interactions are also discussed with respect to the 2C9 crystal structure (*14*).

[1] Abbreviations: 3D-QSAR, three-dimensional quantitative structure−activity relationship; bzbr, benzbromarone; CoMFA, comparative molecular field analysis; CoMSIA, comparative molecular similarity indices analysis; CYP, cytochrome P450; ESI-MS, electrospray ionization mass spectrometry; GC−MS, gas chromatography and mass spectrometry; NSAIDs, nonsteroidal anti-inflammatory drugs.
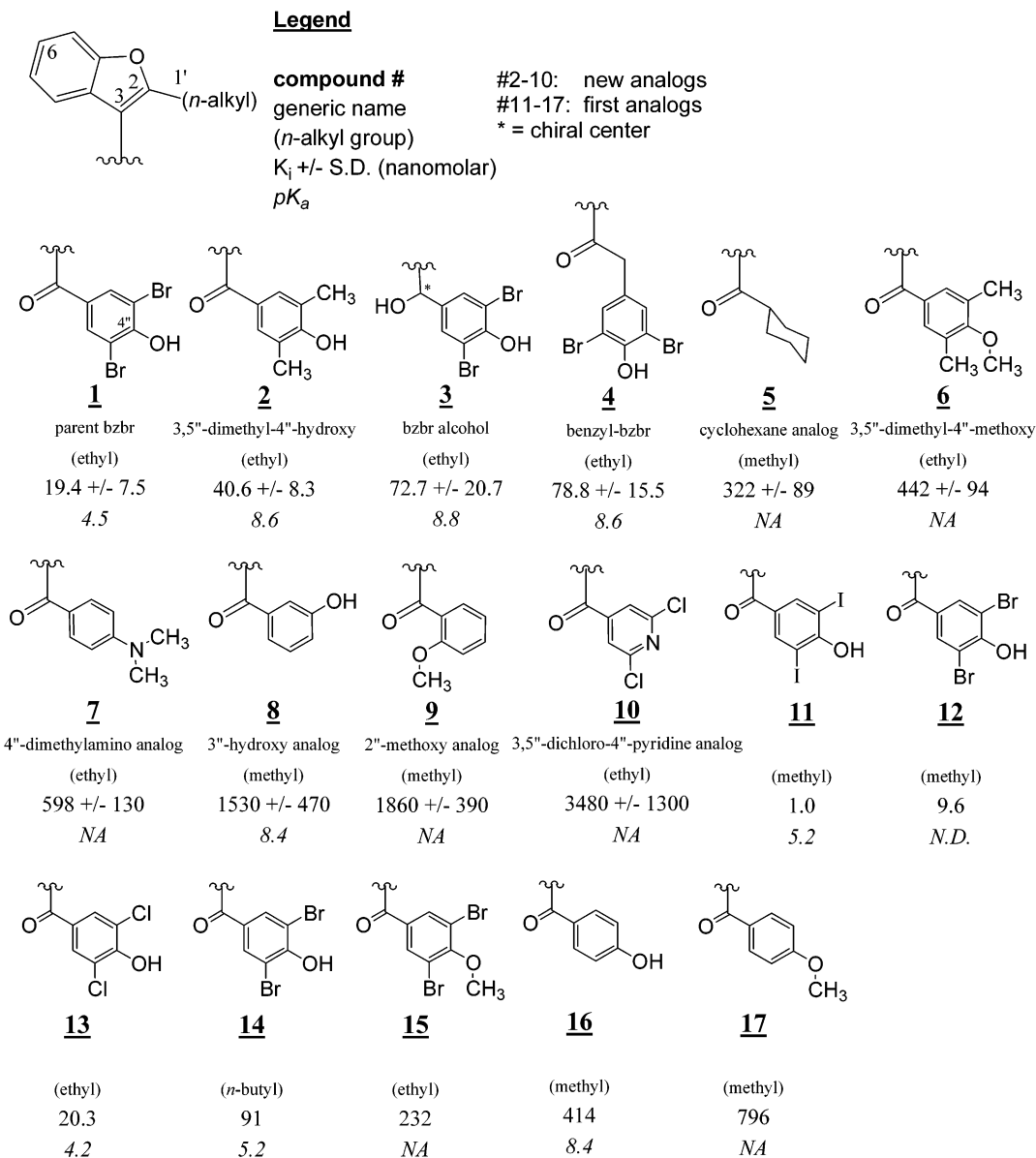
FIGURE 1: Structures and properties of bzbr analogues used in all models.

EXPERIMENTAL PROCEDURES

Chemicals. Fine chemicals were purchased from Sigma-Aldrich (St. Louis, MO), Acros (Morris Plains, NJ), and Lancaster Synthesis (Windham, NH). Solvents were from Fisher Scientific Co. (Pittsburgh, PA) and J. T. Baker (Phillipsburg, NJ).

Protein Purification, Warfarin Metabolite Assay, and pK$_a$ Determination. Detailed methods regarding protein preparation, hydroxywarfarin analysis, pK$_a$ determination, and data fitting can be found in Locuson *et al.* (*15*). Briefly, native human 2C9 was expressed from *Spodoptera frugiperda* (Sf9), purified, and reconstituted into uniformly sized liposomes with purified cytochrome P450 reductase and cytochrome b$_5$, which were expressed in *Escherichia coli*. C-7 hydroxylation of (*S*)-warfarin by the reconstituted enzymes was assessed by GC−MS (*16*). The pH of all enzyme incubations was 7.4. Acid dissociation constants were determined by adding the phenolic inhibitors to 0.1 M potassium phosphate buffer prepared at pH values ranging from 2.0 to 12.0 and monitoring the appearance of phenolate in either the 300 nm

(analogues **3** and **4**) or 350 nm regions (all other acidic analogues).

K$_i$ Determination. Inhibition constants were obtained by keeping (*S*)-warfarin concentrations constant and varying the amount of inhibitor which was used at three or more concentrations. It is important to note that K$_i$ values for bzbr analogues were derived with only one substrate, (*S*)-warfarin, for consistency. It is likely that other substrates will give different K$_i$ values with microsomal P450s, especially those that give rise to atypical kinetics. Nevertheless, a K$_i$ value is still one of the most informative binding constants because it considers the proportional occupancy of binding sites by both the substrate and inhibitor.

A second note should be made regarding the use of kinetic models. To obtain a concentration of inhibitors that is less than the K$_i$, the steady-state assumption that the free substrate concentration is not affected by binding to the enzyme was not valid for some inhibitors. For K$_i$ values near or less than the concentration of P450 (20 nM), inhibitor concentrations will be overestimated. No corrective factors in the competi-

tive inhibition equation or non-steady-state treatment were used. Therefore, the very low K_i values will not be true K_i values. The true K_i values would be even lower. An example of the data fit to the competitive inhibition model is provided as Supporting Information.

Physical Measurements. NMR spectra were collected on a Varian Mercury 300 MHz instrument with $CDCl_3$ as the solvent.

Synthesis. All compounds (Figure 1) were synthesized by acylation of benzofurans with the respective acid chloride using an $AlCl_3$ catalyst. Compounds **4**, **5**, **8**, and **9** were synthesized and purified over silica gel as previously described (*15*). The acid chlorides for compounds **2**, **6**, **7**, and **10** were generated using trichloroacetonitrile and triphenylphospine as reported by Jang *et al.* (*17*). Generally, synthesis was carried out on a 1.0 or 2.0 millimole scale. First, the respective benzoic acid was added to 5 mL of toluene or CH_2Cl_2 and 2.0 equiv of trichloroacetonitrile under argon at room temperature. This was followed by the slow addition of 2.0 equiv of triphenylphosphine in 1 mL of the same solvent and stirring for an additional 10 min. The 2-methyl- or 2-ethylbenzofuran (1.0 equiv) was added followed by 2.0 equiv of anhydrous $AlCl_3$, and the mixture was stirred until the majority of the benzofuran had reacted as monitored by TLC. The workup method used before purification in each case involved quenching the reaction with an ice/water mixture, extracting with ether, drying over $MgSO_4$, and distilling away the solvent and/or concentrating, unless otherwise noted. Purification was carried out with 60−200 mesh silica gel after every step. A few purified compounds, as judged by TLC, NMR, and MS, were obtained as oils that only crystallized upon long-term refrigeration. Those that readily formed solids were recrystallized from hexanes and CH_2Cl_2. The double prime nomenclature used for the benzoyl ring of bzbr follows the literature precedent (*18*).

3,5″-Dimethyl-4″-hydroxy Analogue (2). Anhydrous $AlCl_3$ (2 equiv) was added to **6** in chlorobenzene at 90 °C and stirred for 2 h. Purification over silica gel was carried out with 20% ether in hexanes and gave a light yellow solid: isolated yield, 85%; mp 118−120 °C; ^{1}H NMR δ 1.33 (t, 3H), 2.82 (s, 6H), 2.87 (q, 2H), 5.16 (s, 1H, OH), 7.24 (m, 2H, ArH), 7.46 (m, 2H, ArH), 7.55 (s, 2H, ArH); Via GC−MS, derivatization with diazomethane gives the same product as **6**.

Benzbromarone Alcohol (3). Bzbr (0.2 g) was added to 1 g of dry silica gel and 1.2 equiv of $NaBH_4$ and ground with a mortar and pestle for 20 min (*19*). The reaction mixture was added directly to a gravity silica column and purified using 20% ether in hexanes to give a white solid. D_2O exchange was used to differentiate the phenol and alcohol carbon protons: isolated yield, 10%; mp 144−146 °C; ^{1}H NMR δ 1.33 (t, 3H), 2.16 (s, 1H, OH), 2.82 (q, 2H), 5.85 (s, 1H, OH), 5.99 (s, 1H), 7.23 (m, 3H, ArH), 7.41 (m, 1H, ArH), 7.55 (s, 2H, ArH); ESI-MS m/z 425.0 (M + 1).

Benzyl-Bzbr Analogue (4). Synthesis was accomplished with 2-ethylbenzofuran and (*p*-acylphenoxy)acetic acid with phenol deprotection and bromination carried out as described above. **4** was purified as a white solid: isolated yield, 35%; mp 112−115 °C; ^{1}H NMR δ 1.36 (t, 3H), 3.17 (q, 2H), 4.19 (s, 2H), 5.89 (s, 1H, OH), 7.34 (m, 2H, ArH), 7.35 (s, 2H), 7.51 (m, 1H, ArH), 7.90 (m, 1H, ArH). Via GC−MS,

derivatization with diazomethane gives the following: m/z 452.05 (M, 1), 278.98 (M − 173, 6), 173.17 (M − 279, 100).

Cyclohexane Analogue (5). The cyclohexane analogue was synthesized using cyclohexane carbonyl chloride and 2-methylbenzofuran. This time, the reaction was quenched after 30 min and the mixture purified over silica with 2% ether in hexanes to give a clear liquid: yield, 95%; ^{1}H NMR δ 1.36 (m, 6H), 1.93 (m, 4H), 2.77 (s, 3H), 3.07 (m, 1H), 7.31 (m, 2H), 7.46 (m, 1H), 7.82 (m, 1H); GC−MS m/z 242.17 (M, 39), 158.97 (M − 83, 100).

3,5″-Dimethyl-4″-methoxy Analogue (6). This analogue was synthesized using the acid chloride of 3,5-dimethyl-*p*-anisic acid. Two products were observed, and the desired product had the lower R_f. Purification was carried out with 2% ethyl acetate in hexanes to give a clear oil: isolated yield, 49%; ^{1}H NMR δ 1.33 (t, 3H), 2.32 (s, 6H), 2.87 (q, 2H), 3.79 (s, 3H), 7.24 (m, 2H, ArH), 7.46 (m, 2H, ArH), 7.55 (s, 2H, ArH); GC−MS m/z 308.18 (M, 15), 173.10 (M − 135, 20), 163.07 (M − 145, 44).

4″-Dimethylamino Analogue (7). This analogue was synthesized using 4-(dimethylamino)benzoic acid and CH_2Cl_2 as the solvent. Purification was carried out over silica with 20% ethyl acetate in hexanes to obtain a yellow solid. The desired product was one of two products observed and had the higher R_f value: isolated yield, 20%; mp 75−76 °C; ^{1}H NMR δ 1.33 (t, 3H), 2.90 (q, 2H), 3.08 (s, 6H), 6.65 (d, 2H, ArH), 7.20 (m, 2H, ArH), 7.44 (m, 2H, ArH), 7.81 (d, 2H, ArH); GC−MS m/z 293.09 (M, 68), 278.02 (M − CH_3, 100), 148.05 (M − 145, 63).

3″-Hydroxy Analogue (8). The 3-hydroxy-bzbr analogue without halogens was synthesized using 2-methylbenzofuran and *m*-anisoyl chloride followed by phenol deprotection with $AlCl_3$ to give a yellow oil: isolated yield, 44%; ^{1}H NMR δ 2.55 (s, 3H), 6.06 (s, 1H, OH), 7.25 (m, 8H, ArH). Via GC−MS, derivatization with diazomethane gives the following: m/z 265.87 (M, 100), 250.06 (M − CH_3, 37), 159.03 (M − 107, 64).

2″-Methoxy Analogue (9). This analogue was synthesized with 2-methylbenzofuran and *o*-anisoyl chloride. White crystals were obtained: isolated yield, 31%; mp 90−93 °C; ^{1}H NMR δ 2.47 (s, 3H), 3.71 (s, 3H), 7.04 (m, 2H, ArH), 7.20 (m, 2H, ArH), 7.46 (m, 4H, ArH); GC−MS m/z 265.66 (M, 100), 251.01 (M − CH_3, 58), 158.89 (M − 107, 61).

3,5″-Dichloro-4″-pyridine Analogue (10). 2-Ethylbenzofuran was acylated with the acid chloride of 2,5-dichloroisonicotinic acid. CH_2Cl_2 was used as the solvent. The major product as judged by TLC was the desired product and was subsequently purified with 10% ethyl acetate in hexanes to give a white solid: isolated yield, 5%; mp 105−108 °C; ^{1}H NMR δ 1.37 (t, 3H), 2.95 (q, 2H), 7.33 (m, 2H, ArH), 7.53 (m, 2H, ArH), 7.55 (s, 2H, ArH); GC−MS m/z 319.02 (M, 70), 173.07 (M − 147, 100).

Alignment. The minimized structures of bzbr analogues resulting from semiempirical calculations could nearly be superimposed with (*S*)-warfarin (Figure 2A). Therefore, bzbr structures were aligned so as to overlie the geometry of (*S*)-warfarin used in our previous models (*13*). The C-6 position of the benzofuran was placed between the C-7 and C-6 positions of the warfarin fused ring because it is the primary aromatic hydroxylation product formed in humans (*18*, *20*). This was followed by minor changes in the torsion angles of the sp^2 carbonyl so that the benzoyl ring of bzbr could be
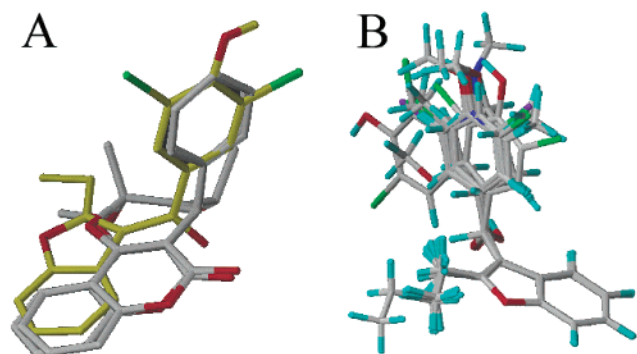
FIGURE 2: (A) Alignment of bzbr (yellow) with (*S*)-warfarin in the ring-opened and ring-closed forms. (B) Complete alignment of 2C9bzbr(17).

FIGURE 3: Representative plot of actual vs predicted ligand activities from the cross-validated neutral 2C9(58) CoMSIA model.

overlaid with the phenyl ring of warfarin. As a result, the ketone oxygen of bzbr nearly overlies the keto oxygen of warfarin. Two compounds that deviated from this template were the bzbr alcohol (**3**) and benzyl-bzbr (**4**) (Figure 1). Since the bzbr alcohol has an sp^3 carbon connecting the two aromatic systems, the aromatic groups are shifted closer to each other. Benzyl-bzbr deviates in the opposite manner with the extra methylene group elongating the distance between the two ring systems. The complete alignment can be visualized in Figure 2B.

Comparative Molecular Field Analysis (CoMFA) and Comparative Molecular Similarity Indices Analysis (CoMSIA) Modeling. CoMFA is one example of ligand-based molecular design software with the ability to derive three-dimensional quantitative structure−activity relationships (3D-QSARs). Using regression analysis on the charges for each atom of each molecule in a three-dimensional aligned library, CoMFA can correlate physicochemical properties with K_i values obtained by experiment. Two utilities of CoMFA analysis are its use as a tool in predicting K_i values of ligands and in constructing contour plots that allow the visualization of predicted favorable and unfavorable properties of the ligands in three dimensions.

Ligands were created with SYBYL version 6.6 (*21*) and minimized using the AM1 Hamiltonian in the included MOPAC module. The resulting structures were then aligned with (*S*)-warfarin as described above, and partial charges were calculated using the MNDO Hamiltonian in MOPAC. All models were obtained using primarily the program defaults with 2.0 kcal/mol column filtering for CoMFA/CoMSIA and an attenuation factor ($\alpha = 0.3$) for CoMSIA. The smallest grid size was the default 2.0 Å block. The inverse natural logarithm of the inhibitor K_i values was used against the various descriptors to generate QSARs using a partial least-squares algorithm. A K_i value is also known as biological activity in a QSAR model, and it was entered as its inverse value so the higher numbers represent higher activities or affinity in this case. The logarithm is taken since the K_i value is related to the CoMFA descriptors (energies) by an exponential relationship.

For models produced from only the 17 bzbr analogues, two forms of the library [2C9bzbr(17)] were used. The neutral library had no formal charges associated with any ligands. An anionic library contained five ligands (**1** and **11**−**14**) that are fully ionized at physiological pH (7.4) according to their pK_a values (Figure 1) and were given a charge of
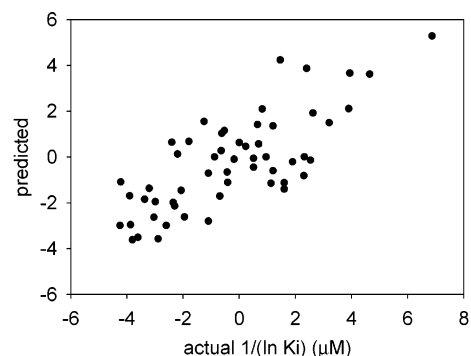
−1. All other bzbr derivatives with phenols had pK_a values greater than 8.3.

Resulting models were only considered meaningful if their cross-validated correlation coefficient r^2 (also known as predictive q^2) exceeded 0.3. Cross-validation weeds out models that merely fit data by testing how well a model predicts the affinity of ligands left out of the data set (*22*). Therefore, a higher q^2 value denotes smaller deviations between actual and predicted affinities and higher potential predictive ability, whereas negative q^2 values denote the opposite. Leave-one-out cross-validation was used in every case to determine the optimal number of components, which was limited to five due to the size of the 2C9bzbr(17) library. q^2 values between 0.38 and 0.75 are reported in Table 1, and a plot of actual versus predicted activities is represented in Figure 3. As an additional test, the K_i values were scrambled randomly two times, and no correlation with activity was made since q^2 was always less than −0.2.

Contour plot levels were viewed between 80 and 90 for favored fields and 20 and 10 for disfavored fields, depending on the size or number of fields. If different fields were blocking each other or were too numerous, the viewing levels were changed to focus on the most prominent fields.

RESULTS AND DISCUSSION

A cationic site or H-bond donor has long been postulated to exist within the active site of CYP2C9 based on the number of acidic substrates that are metabolized. For instance, there is a distinct structural similarity between the NSAIDs (e.g., ibuprofen, flurbiprofen, and naproxen) carboxylate group in relation to the site of metabolism (*7*). Several studies have aimed to locate and better define such a feature since a definitive property like this helps explain the biochemistry of 2C9 and other CYPs that possess wide substrate specificity. It was previously hypothesized that bzbr, the most potent 2C9 inhibitor reported in the literature, derives its potency from being an anion near physiological pH 7.4. The combination of two halogens and a ketone on the phenol ring lowers the pK_a of the phenol to less than 5.2, and therefore, bzbr exists as a phenolate anion, at least in solution. As evidence of the importance of the anion, the affinity of analogues with the acidic phenol hydrogen replaced with a methyl group (**17**) or with a pK_a above 8.3 (**16**) was markedly decreased. Two additional features revealed by constructing bzbr analogues were a preference for small side chains on the benzofuran ring and a second role for the halogens to provide steric bulk or hydrophobicity.

Table 1: CoMFA and CoMSIA Model Statistics

descriptor	fraction[a]	$q^{2\ b}$	r^2	components	standard error (ln)[c]
		Anionic Library[d]			
CoMFA					
electrostatic/steric	0.46/0.54	0.494	0.942	3	0.591
CoMSIA					
electrostatic/steric	0.77/0.23	0.484	0.917	3	0.708
electrostatic		0.564	0.930	5	0.679
steric		negative			
hydrophobicity		0.536	0.708	2	1.23
electrostatic/hydrophobicity	0.56/0.44	0.606	0.942	4	0.593
		Neutral Library			
CoMFA					
electrostatic/steric	0.40/0.60	0.542	0.985	5	0.324
CoMSIA					
electrostatic/steric	0.77/0.23	0.611	0.986	5	0.301
electrostatic		0.578	0.928	5	0.688
steric		negative			
hydrophobicity		0.529	0.724	2	1.19
electrostatic/hydrophobicity	0.55/0.45	0.601	0.974	5	0.413
		Large Library 2C9(58)			
CoMFA					
electrostatic/steric	0.58/0.42	0.643	0.847	4	0.910
CoMSIA					
electrostatic/hydrophobicity/steric	0.41/0.42/0.17	0.752	0.894	4	0.868

[a] Fraction of descriptors that best described the model when more than one was used. [b] As q^2 approaches unity, the $K_{i,predicted}$ is closer to the $K_{i,actual}$, so this value, unlike r^2, partly reflects the predictive ability of cross-validated models. [c] Expected error in K_i predictions in natural log units. [d] The five compounds with pK_a values of ≤ 5.2 were entered into the models with a charge of -1.

With this information, the most potent 2C9 inhibitor, 2-methyl-3-(3,5-diiodo-4-hydroxybenzoyl)benzofuran (**11**), was synthesized and characterized to have a $K_{i,app}$ of 1.0 nM against (*S*)-warfarin. In this study, we have expanded the number of bzbr analogues. The first reason is to develop better nonanionic isosteres of bzbr to further test the anionic binding site hypothesis. Simply stated, since 2C9 substrates are anionic, then 2C9 would have an H-bond donor or other positively charged group to complement negatively charged substrates. The second reason for making bzbr analogues was to develop 3D-QSARs for (1) predicting the binding affinity of untested compounds as a screen for drug–drug interactions and (2) using the predicted specificity determinants as a probe for important substrate–P450 interactions.

Modeling Methodology. Nine new bzbr analogues (**2–10**) (further details below) were synthesized to probe 2C9 specificity (Figure 1). This expanded our initial series of bzbr analogues to 17 compounds. Most new compounds have affinities lower than the original eight with some K_i values reaching into the low micromolar range, but many of the K_i values are not far from that of sulfaphenazole ($\sim$200–300 nM) (*13, 23*), the most potent 2C9 inhibitor reported before bzbr (*24*). In actuality, the range of affinities was beneficial since it provided more depth to the activities of the bzbr data set by expanding the K_i range to exceed 3 orders of magnitude. Because the first step in a 3D-QSAR study, determining biological activity (i.e., K_i values), was completed with a sufficient range of K_i values, the bzbr derivatives were next tested for the ability to create a 3D-QSAR that connects the tight binders (i.e., borderline picomolar K_i) to the weaker binders such as sulfaphenazole and beyond.

CoMFA 3D-QSARs from a Small Bzbr Library. Part of the power of CoMFA (and CoMSIA) comes from the ability to visualize the results of a given model as a contour plot

(Figures 4 and 5). These plots show polyhedron-shaped fields in three dimensions around the periphery of the tested ligands. The colors of these interaction sites show where steric bulk is favorable (green) or unfavorable (yellow) and electron density is favorable (red) or unfavorable (blue) on the ligands.

Overall, electrostatic and steric features each contribute almost equally to describing the generated models (Table 1), but it was thought that since four of the five tightest binders were anionic, the anionic library would provide the best model. In fact, this held true until the trio of less acidic analogues (**2–4**) with affinities closer to that of bzbr were entered into the models, at which point charge state was unnecessary for generating models. Predictive accuracy was actually better for the neutral CoMFA model according to the standard errors (Table 1). The final CoMFA models from both versions of the library placed electropositive fields (blue) near the phenol hydrogen, indicating a preference for less electron density here (Figure 4A,B). This was unexpected since negative charge near the phenol oxygen was thought to increase affinity. Instead, both models predict favorable electron density (red) elsewhere around the benzoyl ring, indicating that the distribution of the negative charge is favorable. In terms of steric interactions, both CoMFA models predict an unfavorable steric interaction (yellow) at the benzofuran C-2 position as suggested by the preference for small side chains in the following order: methyl > ethyl > butyl (Figure 4A,B). The main difference in sterics is the well-defined favorable (green) and unfavorable (yellow) steric interaction adjacent to the phenol in the anionic model that is less defined in the neutral model (Figure 4A,B).

CoMSIA 3D-QSARs from a Small Bzbr Library. The specific CoMSIA descriptors (electrostatic, steric, and hydrophobicity) were evaluated separately and in combinations to see how the results differed from the results with the
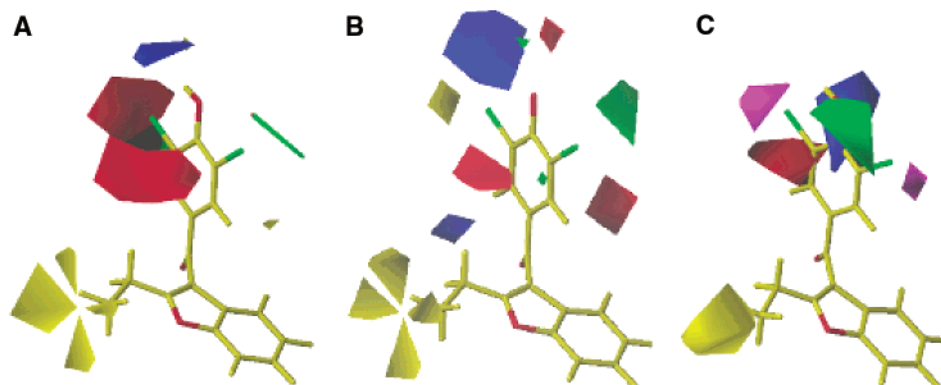
FIGURE 4: Contour plots of CoMFA and CoMSIA models derived from 2C9bzbr(17). The color scheme is as follows: green and yellow for favorable and unfavorable steric interactions, respectively, red and blue for favorable and unfavorable electron density, respectively, and magenta for favorable hydrophobicity. (A) Neutral CoMFA model. (B) Anionic CoMFA model. (C) Neutral CoMSIA model with electrostatics, hydrophobicity, and steric descriptors.
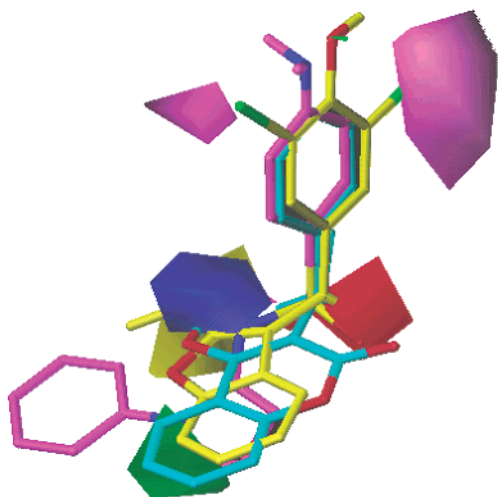

FIGURE 5: Contour plot of the neutral CoMSIA model derived from the 58-compound library. Bzbr is yellow, warfarin cyan, and sulfaphenazole magenta. Hydrophobicity (magenta fields) and the unfavorable steric interaction at the benzofuran side chain (yellow, in the rear) remain important in a more diverse library. Favorable electron density on the bzbr ketone (red) is thought to be a key property underlying most 2C9−substrate interactions and is predicted for the first time.

CoMFA models. In contrast to those of CoMFA, CoMSIA's fields are generated from similarity indices instead of Lennard-Jones and Coulombic potential energies (*25*). This is useful since similarity indices can be adapted to describe several properties in addition to electrostatics and sterics such as hydrophobicity, a descriptor not available with CoMFA. Molecular similarity is also generally thought to provide more contiguous, easily interpretable fields because a Gaussian-type function is used in their construction. The color scheme in the CoMSIA contour plots (Figure 4C) is the same used for CoMFA (Figure 4A,B) with the addition of magenta used to denote hydrophobicity.

CoMFA suggested electrostatics contributes 40−46% and sterics contributes 54−60% to the affinity of the bzbr analogues. To test whether the isolated descriptors arrived at the same answer, the same libraries were subjected to CoMSIA analysis. CoMSIA models made from the neutral and anionic 2C9bzbr(17) libraries produced the best QSARs (leave-one-out $q^2 > 0.3$) by combining electrostatics and hydrophobicity as opposed to electrostatic and steric proper-

ties. No significant advantage over the CoMFA models was observed with respect to q^2 values, though the neutral models are expected to have better predictive accuracy based on their lower standard error (Table 1). In addition, only one insightful result was gained from the contour plots, and that was the positioning of favorable hydrophobic interactions (magenta) above the area corresponding to both bromines of bzbr (Figure 4C). As with CoMFA, the locations of predicted electrostatic interactions were not readily interpretable in terms of a 2C9 pharmacophore as the electropositive (blue) and electronegative (red) sites did not correspond to any particular moiety in any of the bzbr analogues (Figure 4C). When the steric descriptor was added, the expected unfavorable steric feature (yellow) at the benzofuran side chain and a favorable steric feature (green) adjacent to the phenol arose in the contour plots (Figure 4C). While the former interaction agrees with both K_i values and the CoMFA models, the latter is less clear since the affinity of compounds with larger groups at the bzbr phenol depends on the presence of the adjacent bulky groups. Overall, the change in model statistics was small and the contribution of sterics to the model small when this property was included in CoMSIA models.

2C9 3D-QSARs from a Larger Library. While the model is potentially useful for predicting K_i values of similar compounds, one must be cautious about interpreting the results from a 17-compound library as a definitive 2C9 pharmacophore. Hydrophobic interactions and steric restraints localized to the bzbr halogens and benzofuran side chain, respectively, appear to be likely. However, the electrostatic interactions making up the other half of these models remain questionable due to their inconsistencies in the contour plots. Much of the discrepancy no doubt lies in the small size of the libraries and the fact that the chemical diversity is limited to the benzoyl phenol ring.

Therefore, bzbr analogues were added to warfarins, sulfaphenazoles, and NSAIDs from our previous library published as 2C9(41) to make a 58-compound library called 2C9(58) (*13*). Bzbr easily overlaid the phenyl rings of the warfarin analogues and sulfaphenazoles with its ketone being in the vicinity with the warfarin C-2 keto oxygen and sulfaphenzole sulfonamide oxygens (Figure 5). In fact, bzbr and sulfaphenazole are both acidic 2C9 ligands that, upon ionization, can delocalize more electron density to these

Scheme 1: Two Resonance Structures of Benzbromarone
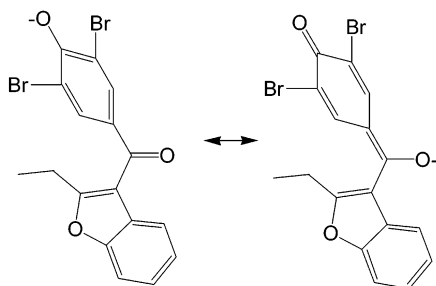
spatially similar oxygens through resonance (Scheme 1). As evidence, the MNDO-assigned partial charge on the bzbr ketone was found to increase upon ionization from −0.28 to −0.35. Sulfaphenazole's oxygens at −0.8 already have the highest charges in the data set in the protonated state. It is tempting to equate the conjugated oxygens in these 2C9 substrates with the role of the carboxylate group in the NSAIDs. One of the reasons warfarin is one of the weaker inhibitors could be its ability to form a hemiketal rather than a resonance-stabilized anion, a phenomenon convincingly demonstrated to occur in the 2C9 active site (*26*). Remarkably, the expanded library CoMSIA model, aligned with the aromatic π-stacking region, electronegative oxygens, and the primary site of metabolism, generated a QSAR that spans an unprecedented range of K_i values, from 48 μM to 1.0 nM. In addition, the final library used only neutral bzbr analogues so knowledge of the charge state was not required.

As with the bzbr models, the CoMSIA models weighted electrostatics and hydrophobicity as being best able to define the K_i data according to q^2 values. When sterics was combined with other descriptors, it always represented the most minor contributor to the models. After models based on the single descriptors and every permutation of descriptors were compared, a representative model with the highest q^2 and the smallest number of components was chosen. This model contained equally contributing electrostatics and hydrophobicity, and a weaker steric contributor.

A contour plot of this expanded CoMSIA model, 2C9-(58), demonstrated a few similarities and differences with the 2C9bzbr(17) library, and gave more insight into the properties of the bzbr benzofuran and ketone regions (Figure 5). An unfavorable steric feature (yellow) was close to the bzbr benzofuran side chain even in this much more diverse data set. A new favorable steric interaction (green) overlaid the site of metabolism. This time, no electrostatic interactions were found in the benzoyl ring, but favored electron density (red) was found near the oxygen-rich area, which corresponds to the bzbr ketone and sulfaphenazole sulfonamide oxygens. Less electron density (blue) was favored around the bzbr benzofuran ring and corresponded to sulfaphenazole's acidic hydrogen. Finally, two hydrophobic interactions (magenta) around the bzbr halogens still remain in the larger model, highlighting the importance of this property.

Important Features of Bzbr Analogues. By pooling the bzbr analogues with diverse groups of warfarin analogues and sulfaphenazoles, we could predict a more logical set of predicted interactions with CoMSIA methods while increasing the predictive range over that achieved with just bzbr analogues. In particular, the predicted interactions account for many observations of bzbr analogues and other substrates

noted in the literature. Each of the new compounds in Figure 1 (**2**−**10**) was synthesized to probe specific features thought to be important in binding to 2C9. Here, the major features of bzbr analogues and other 2C9 substrates are analyzed according to the 2C9(58) model shown in Figure 5.

One of the most frequently mentioned properties of 2C9 substrates, including bzbr, is their acidity. Three novel bzbr analogues (**2**−**4**) closer in structure to the parent bzbr were synthesized to further test the role of the phenol pK_a. Each compound had a pK_a that was at least 3 units higher than those of the anionic analogues and closely retained the steric features of bzbr. The best isostere is the 3,5-dimethylphenol (**2**) whose only difference is substitution of the electron-withdrawing bromines with methyl groups with almost identical van der Waals radii. When bzbr is reduced to an alcohol (**3**), the ketone's absence is responsible for increasing the pK_a of the phenol. The benzyl derivative (**4**) places a methylene carbon between the ketone and phenol ring, thereby insulating the phenol from the ketone. The major difference with these compounds is the preservation of the favorable bulky groups adjacent to the phenol. Because the previous nonacidic analogues for bzbr were much poorer binders than bzbr, it was thought that these three less acidic analogues that preserved the surrounding bulky substituents would have higher affinity. The compounds did have increased potency over the bzbr analogue with a methyl-blocked phenol (**17**) or the bzbr analogue without halogens (**16**). In fact, these better isosteres of bzbr have only 2−4 times higher K_i values than bzbr with pK_a values more than 3 units higher (>8.5). This means they are less than 10% ionized in solution under reaction conditions at pH 7.4. It appears that decreased phenol acidity of **2**−**4** was only slightly deleterious to their activity, while bulky substituents on the same aromatic ring were quite favorable.

While the anionic bzbr derivatives still remained the most potent 2C9 inhibitors, albeit by a minimal margin, the CoMSIA model did not predict any electronegative group near the phenol oxygen even though charge features accounted for half of the model. Yet the 2C9(58) CoMSIA model did predict a favorable electronegative interaction at the bzbr ketone, which aligned closely with the oxygens of sulfaphenazole and warfarin (Figure 5). Hence, the quantitative model agrees with the observation that a similarly placed electronegative group, not necessarily from an ionized substrate, is favored. The fact that bzbr and sulfaphenazole can delocalize more charge onto their oxygens through resonance in the ionized state may give them an edge over warfarin, which likely binds as the ring-closed, hemiketal tautomer to 2C9 (Figure 6). Even **16**, though not very acidic, shows increased affinity over new compound **8**, which is unable to delocalize electron density to its ketone because of its *meta*-positioned phenol. Such an interaction with this specific oxygen was noted in a recent publication for human P450 2C9 (*14*). (*S*)-Warfarin was cocrystallized into a hydrophobic pocket some distance from the heme where the 2-keto oxygen is accepting an H-bond from the backbone amide of F100. On the basis of these considerations, a scheme whereby the ketone of bzbr accepts an H-bond from backbone amide nitrogens or another positively charged site is consistent with the literature and predicted by the atomic charges used to derive the CoMSIA model.
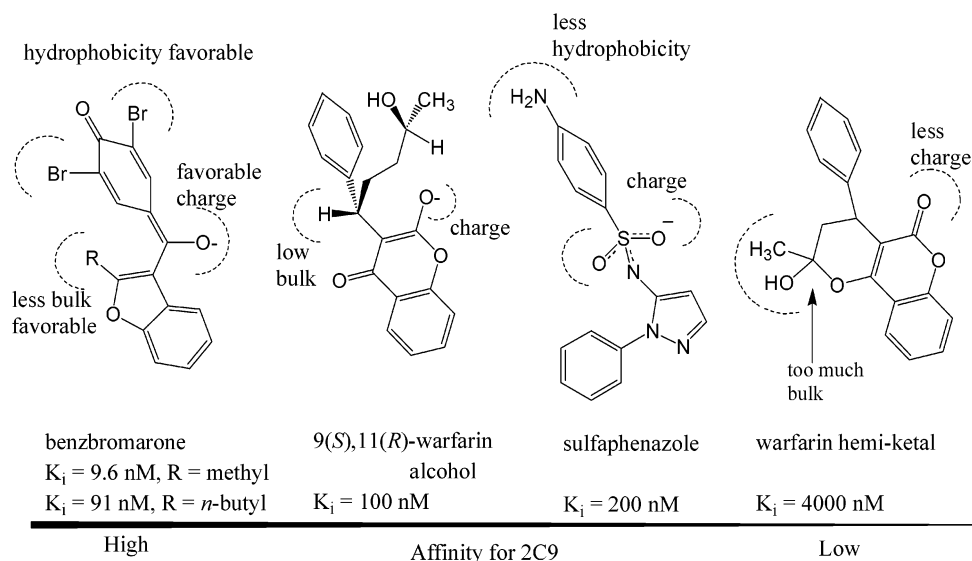
FIGURE 6: Conceptual arrangement of various 2C9 ligands in which relative affinity is explained in terms of bzbr properties.

An electropositive interaction was predicted just above the bzbr benzofuran and, after closer examination, best overlaps the sulfaphenazoles' acidic sulfonamide hydrogens. Although this can be interpreted as a region that corresponds to a negative charge or H-bond acceptor in the enzyme, this result may reflect more the polarizability of groups in this area. More polarizable compounds are better able to put negative charge on the oxygen for an interaction with the enzyme.

Hydrophobic interactions (magenta) are equally important to electrostatics as judged by the model statistics. Hydrophobicity could produce cross-validated models on its own (Table 1). The strong dependence and distinct placement of hydrophobic interaction sites over the bzbr halogens suggest these substituents play a key role in binding. All halogenated bzbr analogues, like the tightest binding diiodo compound (**11**), support this, as does a recent study by Egnell *et al.* (*27*), which predicts two hydrophobes in the 2C9 heteroactivator binding site. Three additional bzbr analogues suggest 2C9 contains a hydrophobic region near the benzoyl ring, which is the location of the aromatic interaction site used in the alignment. Analogue **5** possesses a simple cyclohexane moiety attached to the ketone and has a K_i lower than the K_i values of several having aromatic rings. The dimethyl phenol methyl ether (**6**) and the 4″-dimethylamino analogue (**7**) have affinities resembling that of the bzbr methyl ether (**15**) and so likely make van der Waals contacts with their bulky substituents as well. Moving a methoxy group from the favorable C-4″ (**17**) to the C-2″ position (**9**) decreases affinity, but it is less clear that this can be attributed solely to a lack of van der Waals contacts since the position of the substituent could alter the conformation of the benzoyl ring.

In the case of 2C9, it appears the hydrophobicity of bzbr is favored for enthalpic reasons. No obvious relationship of logP or logD with any specific range of K_i values was found in a two-dimensional plot, and the logP and logD values only deviated by ~2 units except for a few compounds that had intermediate activities (data not shown). If it is true that there is no correlation between the bzbr lipophilicities and their affinity, then most of the favorable steric interactions in the CoMFA models are really favorable hydrophobic interactions with specific sites on the enzyme as predicted by CoMSIA.

Steric features were minor components in defining the data set in CoMSIA models, but display parallels between bzbr and warfarin analogues. Sterics alone were incapable of generating any QSAR as evidenced by negative q^2 values, and the electrostatic/steric model contributed less to sterics (21%) (Table 1). In addition, all permutations of descriptors that included sterics weighted it as the most minor component in explaining the data. Nevertheless, an unfavorable steric interaction at the side chain of the benzofuran (C-2) was found in both models based on the small bzbr(17) library and the larger 2C9(58) library. In the smaller data set, this finding is likely due to a preference for small side chains in this position of bzbr (compare **12** to **14**). In the larger data set, sulfaphenazoles have no steric bulk here. Conversely, select forms of warfarin may contribute to this prediction. The highest-affinity warfarin-like compounds are the phenprocoumon isomers, dicoumarol, and the 9(*S*),11(*R*)-warfarin alcohol (Figure 6) (*13*). Phenprocoumons, lacking the acetyl group of warfarin, have the smallest side chain at the predicted sterically restricted site and bind with a K_i almost 10 times lower than that of warfarin. Dicoumarol lacks this side chain altogether and binds with an affinity similar to that of phenprocoumon. The C-11 warfarin alcohols are incapable of forming the hemiketal structure, but only one diastereomer seems to be able to take advantage of being anionic due to steric differences. The 9(*S*),11(*R*) isomer has a K_i of 0.1 μM, while the 9(*R*),11(*R*) isomer has a K_i of 37 μM. With the substrate alignment described above, it appears the side chain of the 9(*R*) isomer is positioned in the unfavorable steric site because of its low activity. No such bias is evident between the smaller side chains of (*R*)- and (*S*)-phenprocoumon.

One issue to consider with using warfarin itself (not the alcohol) to address steric arguments is the fact that the recently determined crystal structure's electron density appears to fit the ring-opened form of warfarin. Although this is in disagreement with He *et al.* (*26*), it is possible this conformation represents a nonproductive binding mode and that the tautomer equilibrium shifts to close the ring during

approach to the heme. Another possibility is that the amino acid substitutions made to the F-helix and F−G loop regions (K206D, I215V, C216Y, S220P, P221A, I222L, and I223L) required to crystallize the enzyme may have created a ring-opened warfarin binding conformation that is an artifact since some of the mutated residues surround the binding pocket. Differences in the solvation of the active site of the mutated enzyme versus the wild-type enzyme would also be expected to alter the structure of warfarin. As a lipophilic environment drives the formation of ring-closed warfarin (*28*), stronger or altered solvation of the active site could keep warfarin in its ring-opened form (*29*).

The CoMSIA 2C9(58) model also contained one favorable steric site, which was located at the site of metabolism (green) (Figure 5). This could represent either a van der Waals interaction with the I helix due to its proximity to the distal heme surface, the heme itself, or a more distant binding mode. For instance, in the 2C9 crystal structure, this region is nearly in contact with F114, a residue that is important for 2C9's warfarin metabolic profile and tight binding of sulfaphenazole (*30*).

The poorest binder of the data set is one exception where the smaller 2C9bzbr(17) library better fits the qualitative steric observations. The dichloropyridine derivative (**10**) differs from bzbr only by having a nitrogen within the aromatic ring at the 4″ position instead of a phenol, yet this must somehow be responsible for increasing the K_i 2 orders of magnitude above that of bzbr. Derivatives **8** and **9** are the next two poorest inhibitors, and all three of these compounds lack a substituent at C-4″. So there appears to be a specific steric requirement at the 3″−5″ positions of the aromatic benzoyl ring, and the models based on the smaller library do predict a favorable steric interaction (green) above this position (Figure 4C).

Application of CoMSIA Models to Enzyme−Substrate Interactions. The recent publication of a crystal structure shows warfarin bound in the ring-opened form in a position far removed from the heme iron and, hence, the oxidizing species (*14*). Warfarin is bound in a hydrophobic pocket comprised of F476, which is π-stacking with warfarin's phenyl ring, with the 2-keto oxygen of warfarin accepting an H-bond from the backbone amide of F100. This is reproduced with bzbr in Figure 7A, which is very similar to warfarin with respect to composition and geometry. The H-bond agrees with the finding that warfarin analogues display highly dependent metabolism profiles based on the presence of the C-2 keto oxygen, regardless of the tautomeric form (*26*). Sulfaphenazole also shares some of the same features: an aromatic ring and similarly positioned electronegative sulfonamide (Figure 5).

Given the positioning of warfarin, this binding mode could not possibly be a catalytically important binding orientation. Even rotation of warfarin is not likely since P367 and L366 would prevent its approach to the heme. This structure is also inconsistent with the metabolically active binding mode in that ring-opened warfarin is bound, while it has been established that metabolism occurs from the ring-closed form (*26*). A number of possibilities could explain this discrepancy with the most obvious being the following. (1) The binding mode in the reported crystal structure is one of two sites in the active site that can bind warfarin. (2) A conformational change converts the enzyme into the metabolically activated
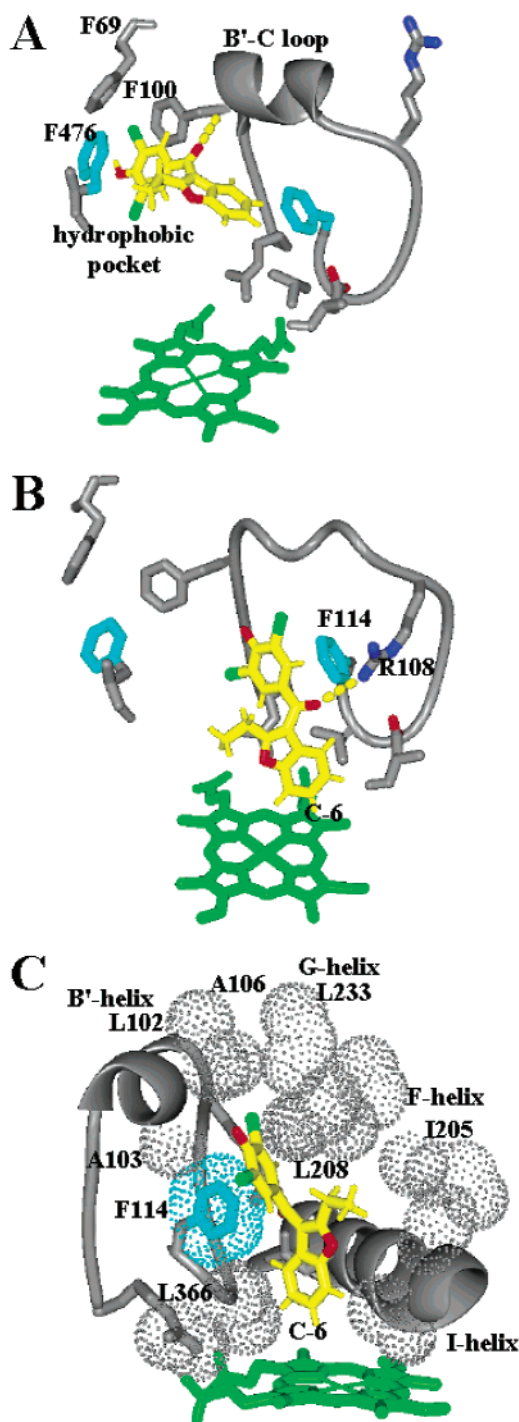

FIGURE 7: Proposed binding modes of bzbr created from Protein Data Bank entry 1OG5 using MidasPlus (*36*, *37*). (A) How bzbr would interact with F476 (cyan) and accept an H-bond from the backbone amide of F100 in analogy to warfarin. (B) In metabolism mode, bzbr could dip toward the heme and switch to an edge-to-face interaction with F114 while ion pairing with R108 on the flexible B′−C loop. (C) The bromines (green) are also capable of making van der Waals contacts with B′, F, and G helix residues in the metabolism binding mode.

conformation. (3) The binding mode represented is an artifact of the mutagenesis of the enzyme needed to make it amenable to crystallization.

With respect to the first point, it is particularly telling that warfarin is the substrate cocrystallized with the enzyme. While ample evidence exists for atypical kinetics and two

substrates binding to 2C9 with a few substrates, warfarin is one of the most studied 2C9 substrates, and no evidence of atypical kinetics has been presented for this substrate. It is possible that the slow turnover of this substrate or fortuitous kinetics obscure the observation of two substrates binding simultaneously; however, given the data available thus far, this is the least likely of the possibilities presented above. Thus, while it is possible that this binding location is involved in the heteroactivation of other substrates such as the activation of flurbiprofen by dapsone (*31*), it seems unlikely that warfarin binds at this location, and then subsequently moves to a catalytically active binding site.

The second possibility that the crystallized structure undergoes a conformational change to a structure responsible for turnover is supported by mutation of R108 and D293, an unpublished crystal structure of 2C9, and the primary structure of the B′−C loop. The R108 residue has been implicated in the binding and/or metabolism of acidic substrates bzbr, diclofenac, flurbiprofen, and warfarin (*32*). Activity toward diclofenac and warfarin metabolism is nearly abolished in R108F mutants where hydrophobic substrate pyrene is unaffected, yet this residue is pointing out into solution in the crystal structure. Another observation is that the overall structure of I helix mutants D293N and D293V is destabilized relative to wild-type 2C9. What is the link between these residues? It turns out that a conformational change allows R108 to form an anion-binding site right near the heme. An unpublished structure presented by E. F. Johnson depicts an unwound B′ helix whose R108 is facing inward, anchored to D293 and interacting with the acidic substrate flurbiprofen (*5, 33*). Therefore, D293 mutants could alter metabolism by decreasing the amount of time the B′−C loop spends forming the R108 anion-binding pocket. The flexible nature of the R108-containing B′−C loop is thought to originate from the primary structure of 2C9 at G96, R97, and G98 and G109, F110, and G111. These two Gly-X-Gly motifs are located on both ends of the B′ helix and appear to be conserved among several members of the 2 family (*34, 35*).

Finally, the same mutagenesis findings and crystallographic information also support the possibility that mutagenesis carried out for crystallization purposes could have produced an artifact. It may be that no substrate motion or B′−C loop movement is required and that the significant mutagenesis around the active site trapped the enzyme in the conformation in which warfarin is bound in the crystal structure. This can be resolved only with further structural studies enlisting other substrates or using enzymes with different or fewer mutations.

A binding pocket positioned above the active heme oxidant is necessary for turnover, but there is at least one other key residue besides R108 that is probably involved in this catalytically active binding mode. Haining *et al.* (*30*) showed that F114, which is closer to the heme than F476, clearly determines the regioselectivity of (*S*)-warfarin metabolism and the high affinity of sulfaphenazole. To illustrate these predicted interactions, when bzbr is modeled into the cationic or metabolizing pocket with F114 pointing at the benzoyl phenol ring in an edge-to-face fashion as in the 2C5− diclofenac structure, an inward facing R108 is within 2.5 Å of the ketone oxygen (Figure 7B) (*35*). Potential contacts for the two bromines are primarily hydrophobic in this binding mode as shown in Figure 7C. This also places the primary aromatic metabolized position (C-6) directly above the heme at ∼3 Å.

If it is assumed that bzbr binds in the more distant binding pocket, it is difficult to reconcile which binding pocket the CoMSIA model describes because each interaction could occur in both locations. Aromatic interactions of F476 and F114 with the benzoyl ring are possible, and the bromines or methyl substituents on the benzoyl ring would be located next to hydrophobic regions in the enzyme at both sites (Figure 7). Both binding sites place the unfavorable steric interaction site for bzbr into a limited but not entirely restricted space either near the region of F476 (Figure 7A) or between the I and F helices (Figure 7C). That leaves the ion pair, but distinguishing between an ion pair like the one envisioned between the ketone and R108 or an H-bond as found in the hydrophobic pocket is complicated by R108 flexibility. It is difficult to measure the more favorable scenario, a solvated R108 residing on the enzyme's surface or the displacement of active site solvent and loss of H-bonds in the B′ helix needed to bring R108 into contact with D293 and substrate. All that is known is that the D293 mutant stabilities described above suggest burying R108's positive charge is favorable.

In conclusion, 3D-QSARs may be useful tools for probing the biochemistry of CYPs. Although often built with the assumption of a catalytically active orientation where the site of metabolism is aligned, they can be used to probe protein structure and how it relates to the substrate binding mode, dynamics, and possibly non-Michaelis−Menten kinetics as observed with dapsone (*31*). As an example, a quantitative CoMSIA model constructed from diverse substrates and a remarkable range of activities suggest that the role of hydrophobicity in 2C9 substrates was underestimated. Electrostatics was an equally good descriptor, and the overlap of a common electronegative site in non-NSAID substrates such as sulfaphenazole, phenytoin, and tolbutamide helped conceptualize a more general 2C9 pharmacophore. Though different results could be produced using a substrate other than warfarin to assess inhibition, the model described here should prove to be useful with its straightforward alignment rules.

SUPPORTING INFORMATION AVAILABLE

An example of (*S*)-warfarin inhibition data fit to the competitive inhibition model. This material is available free of charge via the Internet at http://pubs.acs.org.

REFERENCES

1. Rendic, S., and di Carlo, F. (1997) Human cytochrome P450 enzymes: a status report summarizing their reactions, substrates, inducers, and inhibitors, *Drug Metab. Rev. 29*, 413−580.
2. Miners, J., and Birkett, D. (1998) Cytochrome P4502C9: an enzyme of major importance in human drug metabolism, *Br. J. Clin. Pharmacol. 45*, 525−538.

3. Rettie, A., Korzekwa, K., Kunze, K., Lawrence, R., Eddy, A., Aoyama, T., Gelboin, H., Gonzalez, F., and Trager, W. (1992) Hydroxylation of warfarin by human cDNA-expressed cytochrome P-450: a role for P-4502C9 in the etiology of (S)-warfarin-drug interactions, *Chem. Res. Toxicol. 5*, 54−59.

4. Strickler, M., Goldstein, B. M., Maxfield, K., Shireman, L., Kim, G., Matteson, D. S., and Jones, J. P. (2003) Crystallographic studies on the complex behavior of nicotine binding to P450cam (CYP101), *Biochemistry 42*, 11943−11950.

5. Johnson, E. F. (2003) Deciphering substrate recognition by drug-metabolizing cytochromes P450, *Drug Metab. Dispos. 31*, 1532−1540.

6. Mancy, A., Broto, P., Dijols, S., Dansette, P., and Mansuy, D. (1995) The substrate binding site of human liver cytochrome P450 2C9: an approach using designed tienilic acid derivatives and molecular modeling, *Biochemistry 34*, 10365−10375.

7. Smith, D., and Jones, B. (1992) Speculations on the substrate structure−activity relationship (SSAR) of cytochrome P450 enzymes, *Biochem. Pharmacol. 44*, 2089−2098.

8. White, R., McCarthy, M., Egeberg, K., and Sligar, S. (1984) Regioselectivity in the cytochromes P-450: control by protein constraints and by chemical reactivities, *Arch. Biochem. Biophys. 228*, 493−502.

9. Rock, D. A., Perkins, B. N., Wahlstrom, J., and Jones, J. P. (2003) A method for determining two substrates binding in the same active site of cytochrome P450 BM3: an explanation of high energy omega product formation, *Arch. Biochem. Biophys. 416*, 9−16.

10. Afzelius, L., Zamora, I., Ridderstrom, M., Andersson, T. B., Karlen, A., and Masimirembwa, C. M. (2001) Competitive CYP2C9 inhibitors: enzyme inhibition studies, protein homology modeling, and three-dimensional quantitative structure−activity relationship analysis, *Mol. Pharmacol. 59*, 909−919.

11. Ekins, S., Bravi, G., Binkley, S., Gillespie, J., Ring, B., Wikel, J., and Wrighton, S. (2000) Three- and four-dimensional-quantitative structure activity relationship (3D/4D-QSAR) analyses of CYP2C9 inhibitors, *Drug Metab. Dispos. 28*, 994−1002.

12. Ekins, S., De Groot, M. J., and Jones, J. P. (2001) Pharmacophore and three-dimensional quantitative structure activity relationship methods for modeling cytochrome P450 active sites, *Drug Metab. Dispos. 29*, 936−944.

13. Rao, S., Aoyama, R., Schrag, M., Trager, W. F., Rettie, A. E., and Jones, J. P. (2000) A refined 3-dimensional QSAR of cytochrome P450 2C9: computational predictions of drug interactions, *J. Med. Chem. 43*, 2789−2796.

14. Williams, P. A., Cosme, J., Ward, A., Angove, H. C., Matak Vinkovic, D., and Jhoti, H. (2003) Crystal structure of human cytochrome P450 2C9 with bound warfarin, *Nature 424*, 464−468.

15. Locuson, C. W., II, Wahlstrom, J. L., Rock, D. A., Rock, D. A., and Jones, J. P. (2003) A new class of CYP2C9 inhibitors: probing 2C9 specificity with high-affinity benzbromarone derivatives, *Drug Metab. Dispos. 31*, 967−971.

16. Bush, E., Low, L., and Trager, W. (1983) A sensitive and specific stable isotope assay for warfarin and its metabolites, *Biomed. Mass Spectrom. 10*, 395−398.

17. Jang, D. O., Park, D. J., and Kim, J. (1999) A mild and efficient procedure for the preparation of acid chlorides from carboxylic acids, *Tetrahedron Lett. 40*, 5323−5326.

18. De Vries, J., Walter-Sack, I., Voss, A., Forster, W., Ilisistegui Pons, P., Stoetzer, F., Spraul, M., Ackermann, M., and Moyna, G. (1993) Metabolism of benzbromarone in man: structures of new oxidative metabolites, 6-hydroxy- and 1′-oxo-benzbromarone, and the enantioselective formation and elimination of 1′-hydroxy-benzbromarone, *Xenobiotica 23*, 1435−1450.

19. Liu, W., Xu, Q., and Ma, Y. (2000) Silica gel promoted solvent-free synthesis of arylcarbinols and ferrocenylcarbinols, *Org. Prep. Proced. Int. 32*, 596−600.

20. Rudi, J., Ittensohn, A., De Vries, J. X., Raedsch, R., Walter-Sack, I., Weber, E., and Kommerell, B. (1991) The in vitro microsomal hydroxylation of benzbromarone by human and rat liver, *Hepatology 14*, 235.

21. *SYBYL*, version 6.6 (2002) Tripos Inc., St. Louis.

22. Cramer, R. D., III, Patterson, D. E., and Bunce, J. D. (1988) Comparative Molecular Field Analysis (CoMFA). 1. effect of shape on binding steroids to carrier proteins, *J. Am. Chem. Soc. 110*, 5959−5967.

23. Mancy, A., Dijols, S., Poli, S., Guengerich, P., and Mansuy, D. (1996) Interaction of sulfaphenazole derivatives with human liver cytochromes P450 2C: molecular origin of the specific inhibitory effects of sulfaphenazole on CYP 2C9 and consequences for the substrate binding site topology of CYP 2C9, *Biochemistry 35*, 16205−16212.

24. Takahashi, H., Sato, T., Shimoyama, Y., Shioda, N., Shimizu, T., Kubo, S., Tamura, N., Tainaka, H., Yasumori, T., and Echizen, H. (1999) Potentiation of anticoagulant effect of warfarin caused by enantioselective metabolic inhibition by the uricosuric agent benzbromarone, *Clin. Pharmacol. Ther. 66*, 569−581.

25. Klebe, G., Abraham, U., and Mietzner, T. (1994) Molecular similarity indices in a comparative analysis (CoMSIA) of drug molecules to correlate and predict their biological activity, *J. Med. Chem. 37*, 4130−4146.

26. He, M., Korzekwa, K., Jones, J., Rettie, A., and Trager, W. (1999) Structural forms of phenprocoumon and warfarin that are metabolized at the active site of CYP2C9, *Arch. Biochem. Biophys. 372*, 16−28.

27. Egnell, A. C., Eriksson, C., Albertson, N., Houston, B., and Boyer, S. (2003) Generation and evaluation of a CYP2C9 heteroactivation pharmacophore, *J. Pharmacol. Exp. Ther. 307*, 878−887.

28. Valente, E. J., Lingafelter, E. C., Porter, W. R., and Trager, W. F. (1977) Structure of warfarin in solution, *J. Med. Chem. 20*, 1489−1493.

29. Heimark, L. D., and Trager, W. F. (1984) The preferred solution conforamtion of warfarin at the active site of cytochrome P-450 based on the CD spectra in octanol/water model system, *J. Med. Chem. 27*, 1092−1095.

30. Haining, R., Jones, J., Henne, K., Fisher, M., Koop, D., Trager, W., and Rettie, A. (1999) Enzymatic determinants of the substrate specificity of CYP2C9: role of B′−C loop residues in providing the π-stacking anchor site for warfarin binding, *Biochemistry 38*, 3285−3292.

31. Hutzler, J., Kolwankar, D., Hummel, M., and Tracy, T. (2002) Activation of CYP2C9-mediated metabolism by a series of dapsone analogs: kinetics and structural requirements, *Drug Metab. Dispos. 30*, 1194−1200.

32. Dickmann, L. J., Locuson, C. W., II, Jones, J. P., and Rettie, A. E. (2004) Differential roles of R97, D293, and R108 in enzyme stability and substrate specificity of CYP2C9, *Mol. Pharmacol. 65* (in press).

33. Johnson, E. F. (2003) 12th North American ISSX Meeting, Providence, RI, Oct 12−16.

34. Wester, M. R., Johnson, E. F., Marques-Soares, C., Dansette, P. M., Mansuy, D., and Stout, C. D. (2003) Structure of a substrate complex of mammalian cytochrome P450 2C5 at 2.3 Å resolution: evidence for multiple substrate binding modes, *Biochemistry 42*, 6370−6379.

35. Wester, M. R., Johnson, E. F., Marques-Soares, C., Dijols, S., Dansette, P. M., Mansuy, D., and Stout, C. D. (2003) Structure of mammalian cytochrome P450 2C5 complexed with diclofenac at 2.1 Å resolution: evidence for an induced fit model of substrate binding, *Biochemistry 42*, 9335−9345.

36. Bash, P. A., Pattabiraman, N., Huang, C. C., Ferrin, T. E., and Langridge, R. (1983) van der Waals surfaces in molecular modeling: implementation with real-time computer graphics, *Science 222*, 1325−1327.

37. Ferrin, T. E., Huang, C. C., Jarvis, L. E., and Langridge, R. (1988) The MIDAS display system, *J. Mol. Graphics 6*, 13−27.